Millimeter-wave Wideband High-isolation Antenna Array Based on End-fire Magnetoelectric Dipole Antenna for 5G Applications

Fang-Fang Fan, Qing-Lin Chen, and Kai Qin

The Key Laboratory of Antennas and Microwave Technology
Xidian University, Xi'an 710071, China
fffan@mail.xidian.edu.cn, 929938860@qq.com, qkqinkai@foxmail.com

Abstract **–** In this paper, a millimeter-wave (mmW) wideband high-isolation wide-angle scanning antenna is presented. The end-fire magnetoelectric (ME) dipole with wideband impedance characteristic and wide beamwidth is selected. Based on the ME dipole, a 1×4 subarray with a stripline feed network is constructed to get higher antenna efficiency. Then, four 1×4 subarrays are adopted to form a 4×4 array to realize the wide-angle scanning performance. Furthermore, to get better isolation between the subarrays, the beam is tilted on the non-scanning plane; in addition, the resonant split rings are added on the background of the subarrays. With these two measures, the isolation between the subarrays can be effectively reduced, with more than 20 dB over the entire bandwidth. Owing to the wide beamwidth of ME dipole and high isolation between the subarrays, the 4×4 array can obtain the wide-angle scanning characteristic. The final antenna covers an operating bandwidth of 19.5% (24.25-29.5 GHz) with return loss more than 10 dB, which can meet the band in the 5G standard. The beam can scan approximately ±55° with a realized gain reduction under 3 dB within the wide operating bandwidth. Also, the simulated radiation efficiency of the array is more than 77% over almost the entire band. The antenna will be a potential candidate to be applied in 5G applications.

Index Terms **–** fifth generation (5G), high-isolation, magnetoelectric (ME) dipole, wide-angle scanning, wide bandwidth.

I. INTRODUCTION

Nowadays, with the rapid development of wireless communication, millimeter-wave (mmW) antenna systems have played an important role and been widely used in mobile communication, driverless cars technology, internet of things and other fields because of its high data rate, low response time and wide operating bandwidth. Promoting the development of the fifth-generation (5G) wireless communication, mmW wideband, high isolation and wide-angle scanning phased array antennas are urgently required, especially those that work in 5G band.

During the past few years, many kinds of wideband mmW antenna arrays based on different structures have been designed, such as tapered slot antenna [1], meta-surface antenna [3–4, microstrip patch antenna [5], quasi-Yagi antenna [6], and horn antenna [7]. However, few of them have wide-angle scanning characteristic and high isolation between the elements at the same time. The literature [8–12] show the excellent scanning performance, such as transmitarrays [8], reflectarrays [9], dielectric resonators [10], and lenses [11]. However, the size of these antennas is not suitable to integrate with other devices. In literature [13–17], the wide-angle scanning performance can be obtained, while the port isolation between the elements is not so desirable with only more than 15 dB, even some methods have been employed to reduce the mutual coupling. Thus, designing an antenna possessing wideband, high isolation and wide-angle scanning is still a challenging task. As for the element, magnetoelectric (ME) dipoles show great advantages of wide bandwidth, wide beamwidth, and superior radiation performance by combining complementary electric dipole and magnetic dipole in mmW band [18, 19].

II. ANALYSIS OF THE ANTENNA ELEMENT AND ARRAY

A. ME dipole element

The array antenna element is designed based on the ME dipole in [20]. It is an end-fire ME dipole with wide bandwidth and wide beamwidth, which is a good candidate for the wide-scanning array element. However, it is printed on a single-layer dielectric substrate with the thickness of 0.254 mm, which is too thin to hold the larger array. Moreover, the microstrip feed network would suffer higher transmission loss in mmW band. Thus, two dielectric substrates are employed to get a stripline structure as the feeding network can be seen in Fig. 1, which can meet the requirements of hard structure and low loss.

In Fig. 1 (a), the upper part in the red dashed frame is electric dipole, and the lower part in the blue dashed frame is a single loop antenna, playing the role of mag-

Submitted On: September 29, 2022
Accepted On: December 10, 2022

https://doi.org/10.13052/2022.ACES.J.371108

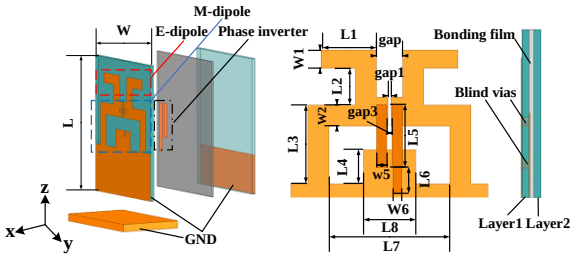

(a) (b)

Fig. 1. Configuration of the element. (a) Perspective view. (b) Front view and side view.

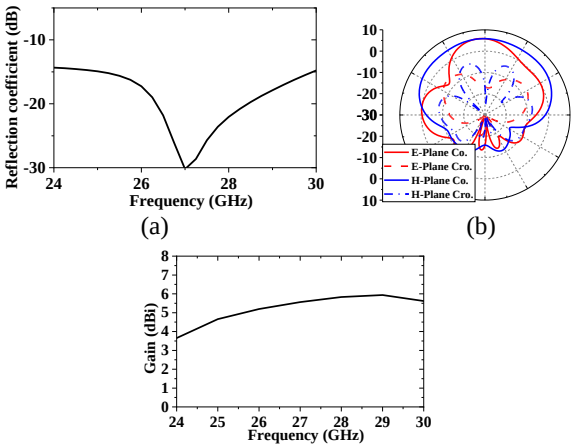

(a) (b) (c)

Fig. 2. Simulated results of the proposed antenna element: (a) reflection coefficient, (b) radiation patterns at 27 GHz, (c) radiation gain.

netic dipole. The two antennas are combined together and are excited by a phase inverter, providing 180° phase shift over a broadband range. The electric dipole and magnetic dipole have different resonant frequencies, which broaden the operating frequency of the total antenna. Both of the two substrates used here are Rogers Duroid5880 substrate with thickness of 0.254 mm. On the backside of layer2, a rectangular conductor acts as the stripline's ground. The horizontal copper plate plays the role of reflecting beam and fixing antenna substrate. From the side view of Fig. 1 (b), a bonding film (Rogers 4450F, εr=3.5, tanδ=0.004) with a thickness of 0.2 mm is used to align the two substrates together. All the dimensions of the ME dipole are marked in Fig. 1 (b). After the mass simulation analysis and optimization, the element exhibits outstanding performance as shown in Fig. 2, over the frequency range of 24-30 GHz, the simulated return loss is larger than 15 dB. The realized gain is more than 4 dBi and the maximum realized gain is up to 5.9 dBi over the band 24.25-29.5 GHz. The simulated realized gain radiation pattern at the center frequency 27 GHz in Fig. 2 (b) shows that the cross polarization in the E-plane and H-plane is higher than 25 dB in the broadside direction. The 3 dB beamwidth is 154° at 27 GHz in H-plane, which is advantageous for wide-angle scanning. That is to say, the two layers substrate ME dipole also can be a good element candidate for the phase array application because of the wide impedance bandwidth and wide beamwidth in H-plane. The dimensions of the element are shown in Table 1.

Table 1: The optimum value of the parameter for the double substrates ME dipole (unit: mm)

Parameter	*w1*	*l2*	*w2*	*l3*	*l4*	*l5*
Value	0.7	2.1	0.8	3	1.3	2.4
Parameter	*l8*	*gap*	*gap2*	*gap3*	*W*	*l6*
Value	2	1	0.12	0.2	7.5	1
Parameter	*L*	*l1*	*l7*	*w5*	*w6*	
Value	9.5	2.1	6.2	0.4	0.34	

In Fig. 2, the parametric study of the ME element has been conducted, we can conclude that the parameters *L3* and *gap* affect the reflection coefficient obviously. And *L3* affects the resonating frequency more than *gap*. The current distribution on the patch also has been given in Fig. 4, it can be seen that the current densities on the dipole attain their maximum strength when t=0. After a quarter of a period, the current densities on the loop attain their maximum, which means that

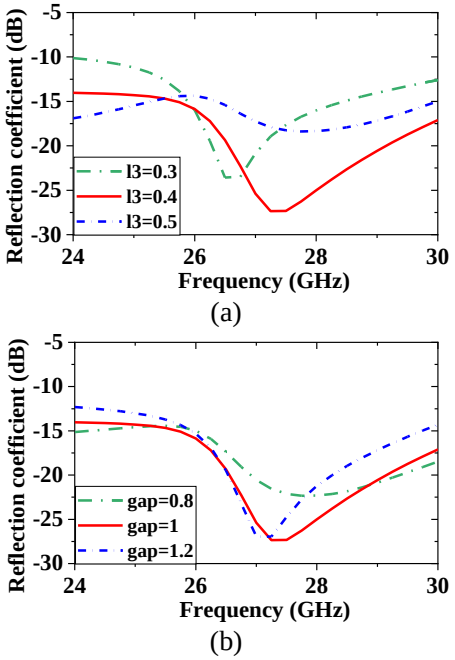

(a) (b)

Fig. 3. Simulated reflection coefficient of different (a) l3, (b) gap.

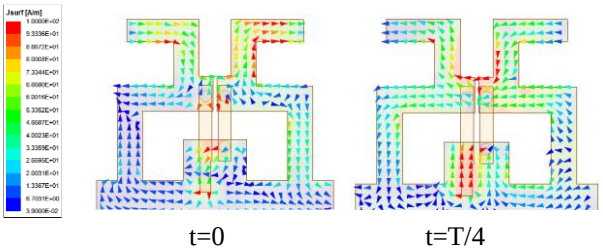

Fig. 4. The current distribution of the antenna element.

the electric dipole and the magnetic dipole are strongly excited.

B. 1×4 array design

Based on the proposed ME dipole, a 1×4 linear array is designed. As shown in Fig. 5, the element distance is set as 7.5mm in E-plane, which is $0.64\lambda_0$ of the center frequency 27 GHz. With this element distance, the mutual coupling between the elements is weak and has little effect on the array performance. In such a compact layout, it is impossible to place the power division network on the ground and feed the antenna through the floor with a probe as the conventional feeding network. Therefore, the power division network and 1×4 linear array are designed on the same dielectric substrate as seen in Fig. 5. The four elements are excited by a 1-to-4 stripline power divider, which has higher efficiency than a microstrip power divider with a single-layer dielectric substrate in the mmW band. In Fig. 6 (a), the impedance bandwidth for |S11|<-20 dB is 24-30 GHz. The highest realized gain is 11 dBi, and the radiation patterns at 27 GHz are given in Fig. 6 (b). We can see that the array exhibits a stable radiation pattern and wide H-plane beamwidth over the operating band.

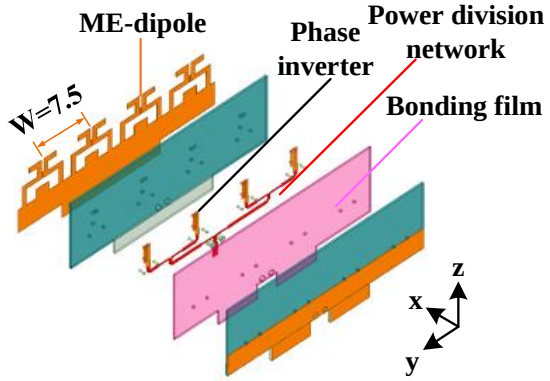

Fig. 5. The geometry of the 1×4 linear array.

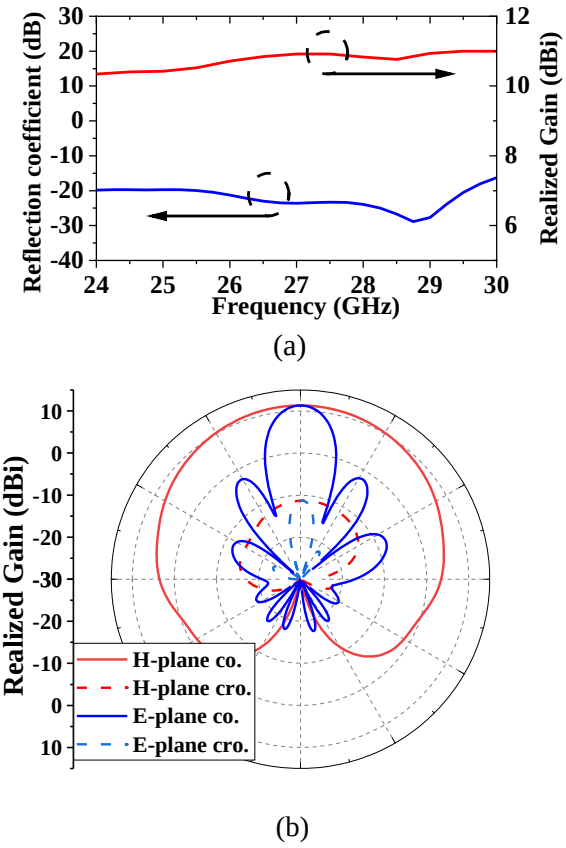

Fig. 6. The simulation results of the 1×4 linear array. (a) reflection coefficient and realized gain, (b) radiation patterns at 27 GHz.

C. 4×4 array with beam-tilt in E-plane

Based on the above 1×4 subarray, four 1×4 subarrays are employed to obtain a 4×4 array. Considering the requirements of isolation and radiation pattern scanning performance, the 4×4 array needs a compact physical structure, so the subarray spacing is 4.8 mm ($0.44\lambda_0$ at 27GHz in the free space) as can be seen in Fig. 7.

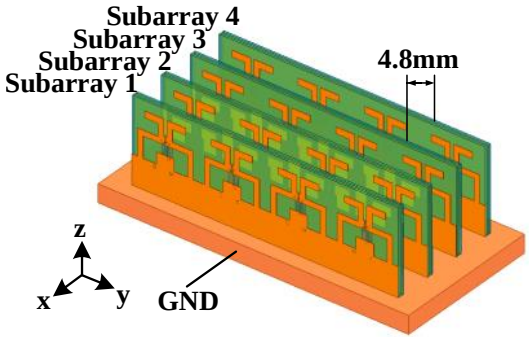

Fig. 7. The structure of the 4×4 array.

As depicted in Fig. 8, the return loss for the four outputs is larger than 12.5 dB over the whole frequency band. However, the isolation between the linear arrays is not so good, especially at lower frequencies. The worst value is about 11 dB, which would deteriorate the scanning performance for the 4×4 array.

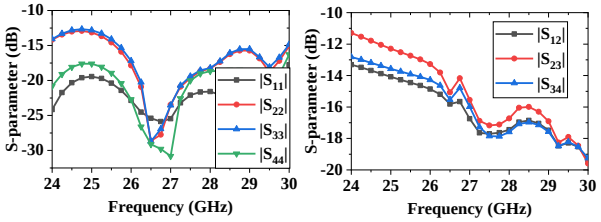

(a) (b)

Fig. 8. The S-parameters of the 4×4 array. (a) Return loss of four outputs. (b) Isolation between the four outputs.

In general, in the wireless communication system, beam tilt is used to expand the covered area and improve the antenna element isolation at the orthogonal plane. Here, this method is adopted to achieve better isolation between the subarrays. The decoupling principle of the beam-tilt design is shown as in Fig. 9, suppose an array composed of 8 elements denoted as A1-A8 can, it can be divided into 2 channels. A1-A4 are the four antennas in channel 1, A5-A8 are the four antennas in channel 2. If the feeding currents on antennas in channel 1 can be denoted as $i_1=e^0$, $i_2=e^{-if}$, $i_3=e^{-i2\varphi}$ and $i_4=e^{-i3\varphi}$, where the amplitude of the current is 1, the phase delay is $-\varphi$ to obtain the scanning characteristic. The phase delay -φ' is caused by the free space coupling path, if other factors can be ignored, then the current at antenna 5 through the coupling from antenna 1 is $e^{-if'}$ the so the received signal at the input port in channel 2 can be obtained as:

$$i_{receive}=e^{-i\varphi'}(1+e^{-i2\varphi}+e^{-i4\varphi}+e^{-i6\varphi}). \quad (1)$$

According to the Euler formula, it can be written as:

$$i_{receive}=e^{-i\varphi'}\begin{matrix}1+\cos2\varphi+\cos4\varphi+\cos6\varphi\\ i(\sin 2\varphi+\sin4\varphi+\sin6\varphi)\end{matrix}. \quad (2)$$

Then the modulus value is:

$$|i_{receive}|=\sqrt{4+6\cos2\varphi+4\cos4\varphi+2\cos6\varphi}. \quad (3)$$

Set phase difference $\varphi=n\pi$, as long as n is not an integer, the modulus of the received signal in channel 2 is less than 4. If $\varphi=0$, then $i'_{receive}=4e^{-i\varphi'}$, $\left|i'_{receive}\right|=4$. When the beam deflects and φ is not equal to the integral multiple of π, that is $|i_{receive}|<\left|i'_{receive}\right|$, it can reduce the coupling between channels.

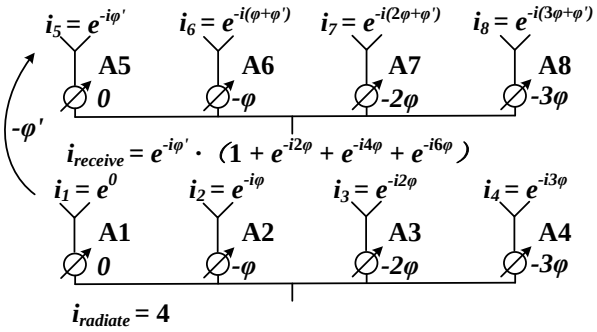

Fig. 9. The decoupling principle of beam-tilt design.

According to the calculation and analysis, the optimum beam down-tile angle should be 8°, which can meet the requirements of the channel isolation in H-plane and the directional gain in E-plane. Therefore, the phase difference between the output ports of the power divider should be 35°.

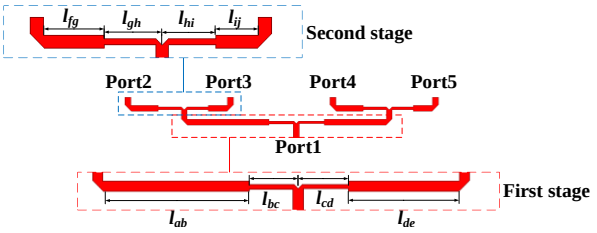

Fig. 10. The diagram of the unequal phase power divider.

The diagram of the unequal phase power divider is shown in Fig. 10. It consists of two stages of power divider. In the first stage, the electrical length of l_{ab} is more than l_{de} by 70° (the physical length is 1.53 mm at 27 GHz) and the electrical length of l_{bc} and l_{cd} is set as a quarter of the wavelength at 27 GHz, the characteristic impedance is 70.7 ohm to determine the width of the strip line. In the second stage, the length of l_{fg} is 0.76 mm longer than l_{ij}, corresponding to a phase difference of 35°. After fine-tuning, the dimensions of the unequal phase power divider are obtained as shown in Table 2.

Table 2: The optimum value for the unequal phase power divider (unit: mm)

Parameter	l_{ab}	l_{bc}	l_{cd}	l_{de}
Value	6.06	2	2	4.52
Parameter	l_{fg}	l_{gh}	l_{hi}	l_{ij}
Value	2	1.9	1.78	1.39

In Fig. 11 (a), the return loss is larger than 20 dB over the whole band. And the transmission coefficients are better than -6.56 dB, which mean the biggest insertion loss is 0.56 dB. The amplitude unbalance is ±0.3dB or so, while the phase unbalance is just ±5°.

With the above unequal phase feeding network, the isolation can be improved obviously. As given in Fig. 2, the coupling between the subarrays has been decreased by 5dB in average. Especially at high frequencies, the isolation even reaches 35dB, compared with Fig. 8 (b).

Additionally, the simulated radiation efficiency has been given in Fig. 13, across the entire band, it is more than 76%.

D. 4×4 array with resonant split rings

For the need of scanning, the 4 × 4 array is placed on a copper ground with a size of 40mm×30mm×2mm.

As shown in Fig. 14, fix the four 1×4 subarrays and connector, the copper ground is slotted. The 1×4 arrays

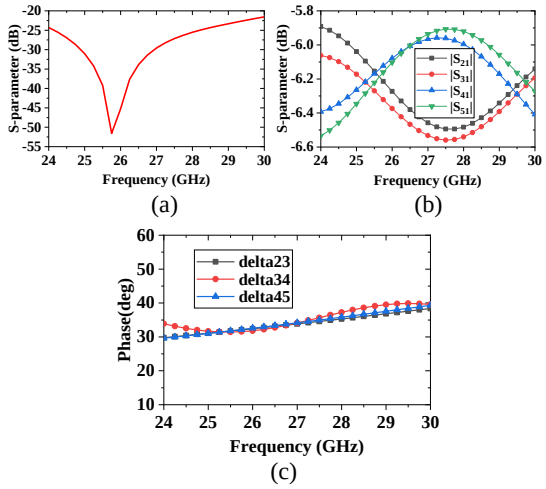

Fig. 11. The simulated results of the unequal phase power divider. (a) Return loss, (b) transmission coefficients, and (c) transmission phase difference.

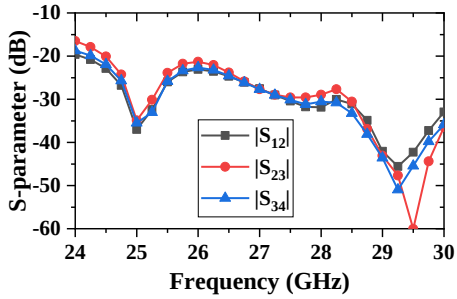

Fig. 12. The isolation between the subarrays with beam-tilt.

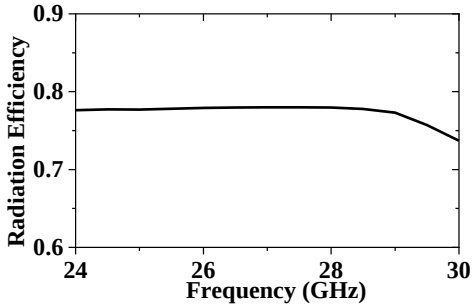

Fig. 13. The simulated radiation efficiency of the array.

are divided into two groups and placed symmetrically for better cross-polarization [21].

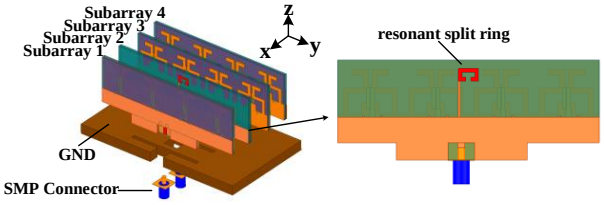

Fig. 14. The final diagram of the 4 × 4 array for fabrication.

The isolation between 2 and 3 channels at approximately 25 GHz is less than 20 dB. To achieve high isolation at lower frequencies, resonant split rings are added to the 4×4 array. Firstly, resonant split rings resonating at 25 GHz are added on the back side of subarray2 and subarray3 to absorb electromagnetic energy. Then the resonant split rings are grounded to transmit energy to the ground through a long thin line. After loading the open resonant ring, the isolation between the subarrays has been improved more than 20dB as given in Fig. 15.

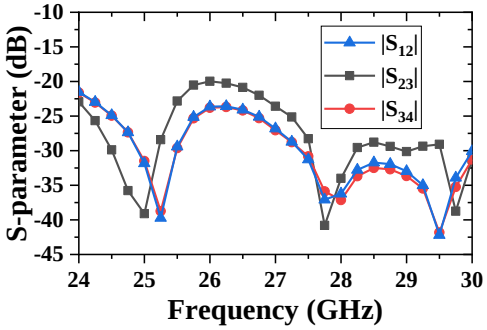

Fig. 15. The isolation between the subarrays with resonant split rings.

E. The wide-angle scanning performance

To verify the beam scanning performance, active simulation cooperated with full-wave solver ANSYS HFSS is implemented. The four 1×4 subarrays are fed by excitations with same amplitudes and different phases. Figures 16 (a)-(b) depicts the simulated active reflection coefficients at the broadside direction and the scan angle of 55°. It can be seen that the active reflection coefficients for four subarrays is less than -10 dB even at the scan angle of 55°, owing to the excellent isolation between the subarrays. The main beam can scan to 55° with scan losses lower than 3.0 dB/2.5 dB and sidelobes lower than -8.5 dB/-4.7 dB at 24.25 GHz/29.5 GHz as shown in Figs. 16 (c)-(d).

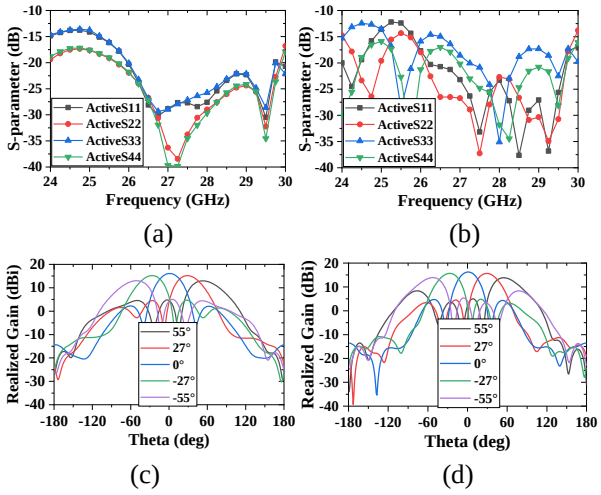

Fig. 16. The Active S-parameters when the beam scan to (a) 0°, (b) 55°, and the wide-angle scanning performance at (c) 24.25 GHz, and (d) 29.5 GHz.

III. MEASURED RESULTS AND DISSCUSION

For verification, a prototype of the 4×4 array loaded with open resonant ring, as shown in Fig. 17, was fabricated and measured. The S-parameters of the array were measured by Agilent E8363B vector network analyzer, and the results are shown in Fig. 18. It can be seen that the return loss is almost higher than 10 dB from 25 GHz to 30 GHz, some points are less than 10 dB owing to the fabrication error, and the isolation between the channels is lower than -20 dB from 24 GHz to 30 GHz.

The radiation pattern of the array is measured by an in-house far-field mmW antenna measurement system, and the gains were measured by comparing with the standard gain horn antenna. Figure 19 gives the measured radiation pattern in H-plane with the one-to-four equal powder divider, we can see the radiation patterns at different frequencies meet with the simulated ones.

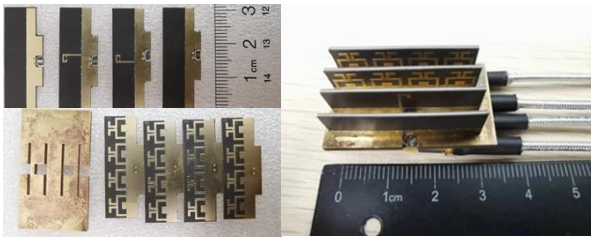

Fig. 17. The photo of the fabricated 4×4 array. (a) the disassembled antenna. (b) the assembled antenna.

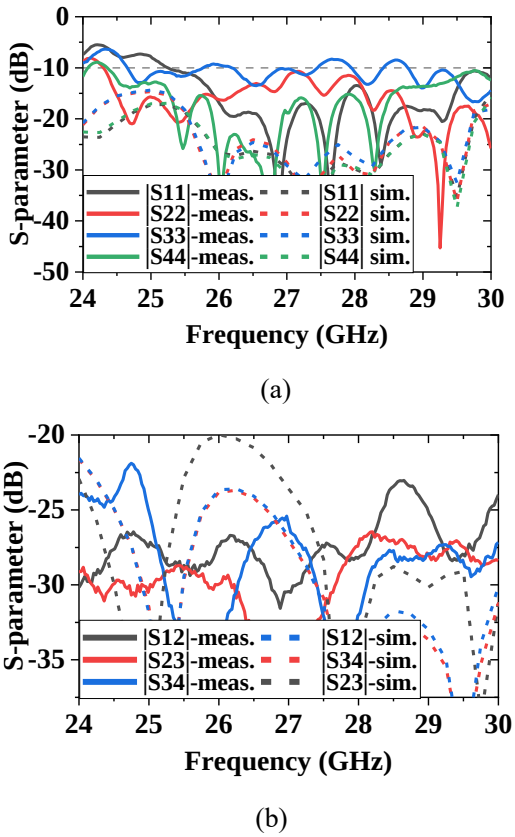

Fig. 18. The simulated and measured S-parameters of the 4×4 array. (a) Return loss. (b) Isolation.

From the E-plane radiation patterns, the beam points to the maximum at about 8°. Unfortunately, there is no suitable beamforming network to verify the scanning performance of the final fabricated array, but it is believed that the scanning performance will be fine as expected, like the above E-plane and H-plane radiation patterns. The simulated and measured gain are compared in Fig. 20, the measured gain is up to 15.0 dBi with a variation of 1.0 dB over the operating band of the array. The deviation between measured and simulated gain results

Table 3: Comparisons with other antenna arrays

Ref	f_0 (GHz)	Bandwidth (%)	Dimension	Isolation (dB)	Scan Range (°)	Size	Gain Loss (dB)
[1]	27	47	1×4	N.A.	±35	1.1 λ_0 × 2 λ_0	3
[14]	27	17.7	1×8	< -15	±62	0.5 λ_0 × 4 λ_0	3
[16]	6.2	11.5	1×4	< -15	±70	0.46 λ_0 × 1.2 λ_0	3
[17]	3.5	28.6	1×8	< -13	±60	0.28 λ_0 × 2.33 λ_0	2.5
This work	27	19.5	4×4	< -20	±55	1.29 λ_0 × 2.5 λ_0	3

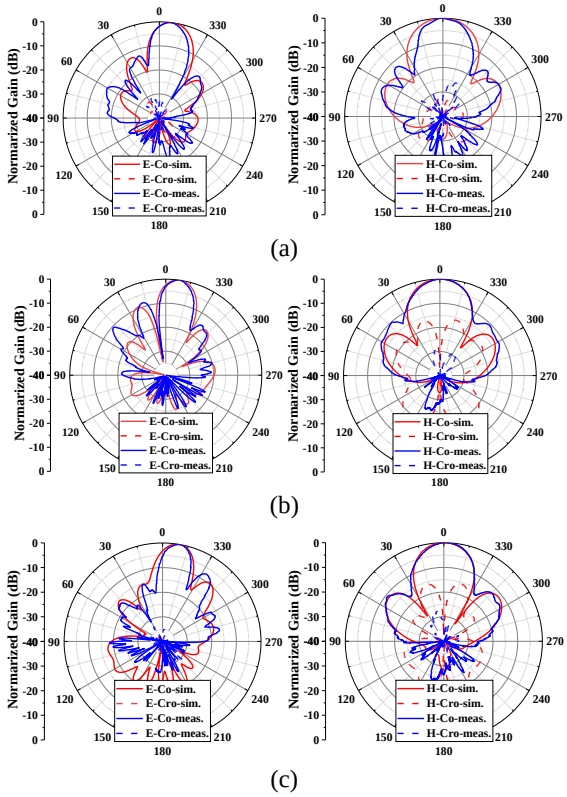

Fig. 19. The measured radiation patterns for the proposed antenna array (Left: E plane Right: H plane) at: (a) 24.25 GHz, (b) 27 GHz, and (c) 29.5 GHz.

is mainly caused by fabrication error and the uncertain influence of the measurement setup close to the antenna under test. The degradation of the impedance matching at the lower band of the frequency range would also affect the measured gain.

In Table 3, the comparison between our work and other antenna arrays is presented. The suggested antenna array has a broader operating bandwidth and higher isolation than the designs in [14] and [16] because of the wide band characteristic of the proposed antenna element and the isolation improvement measures for the array. The bandwidth of antenna in [1] is much wider than the proposed antenna, while our work has better performance in beam scanning. The array in [17] has wide-angle scanning and wideband characteristic; however, the isolation between the subarrays is not as good as our work.

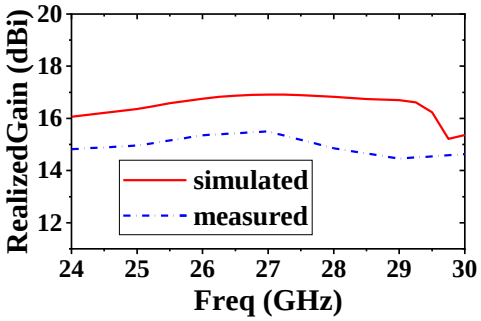

Fig. 20. Measured and simulated peak gain of the proposed antenna array.

IV. CONCLUSION

A mmW wideband high-isolation wide-angle scanning phased array based on end-fire magnetoelectric (ME) dipole is presented. A 1×4 double dielectric substrate planar ME dipole linear array with a strip line feed network is designed to get higher antenna efficiency. Then, four 1×4 subarrays is used to form a 4×4 array to realize the wide-angle scanning performance. Furthermore, to achieve better isolation, both beam down-tilt and resonant split rings are employed. Owing to the wide beamwidth of ME dipole and high isolation between the subarrays, the 4×4 array can obtain the wide-angle scan characteristic. The final antenna covers an operating bandwidth of 19.5% (24.25-29.5 GHz) with return loss more than 10dB, which can meet the band in the 5G standard. The mutual coupling between the subarrays can be effectively reduced less than -20dB over the

entire bandwidth. The beam can scan of approximately $\pm 55^{\circ}$ with a realized gain reduction under 3 dB in the wide operating bandwidth. Additionally, the simulated radiation efficiency of the array is more than 77% over almost the whole band. The antenna will be a potential candidate to be applied in 5G applications.

REFERENCES

[1] B. Yang, Z. Yu, Y. Dong, J. Zhou, and W. Hong, "Compact tapered slot antenna array for 5G millimeter-wave massive MIMO systems," *IEEE Trans. Antennas Propag.*, vol. 65, no. 12, pp. 6721-6727, 2017.

[2] T. Li and Z. N. Chen, "Wideband sidelobe-level reduced Ka-band metasurface antenna array fed by substrate-integrated gap waveguide using characteristic mode analysis," *IEEE Trans. Antennas Propag.*, vol. 68, no. 3, pp. 1356-1365, 2020.

[3] S. P. Dubazane, P. Kumar, and T. J. O. Afullo, "Metasurface superstrate-based MIMO patch antennas with reduced mutual coupling for 5G communications," *Applied Computational Electromagnetics Society (ACES) Journal*, vol. 37, no. 4, pp. 408-419, 2022.

[4] H. Zhu, Y. Qiu, J. Bai, and G. Wei, "Compact design of non-uniform meta-surface for patch antenna main beam steering," *Applied Computational Electromagnetics Society (ACES) Journal*, vol. 34, no. 9, pp. 1300-1304, 2019.

[5] D. Wang, H. Wong, K. B. Ng, and C. H. Chan, "Wideband shorted higher-order mode millimeter-wave patch antenna," *Proceedings of the 2012 IEEE International Symposium on Antennas and Propagation*, pp. 1-2, 2012.

[6] L. Lu, K. Ma, F. Meng, and K. S. Yeo, "Design of a 60-GHz Quasi-Yagi antenna with novel ladder-like directors for gain and bandwidth enhancements," *IEEE Antennas Wireless Propag. Lett.*, vol. 15, pp. 682-685, 2016.

[7] Y. Li, L. Ge, J. Wang, S. Da, D. Cao, J. Wang, and Y. Liu, "3-D printed high-gain wideband waveguide fed horn antenna arrays for millimeter-wave applications," *IEEE Trans. Antennas Propag.*, vol. 67, no. 5, pp. 2868-2877, May 2019.

[8] P.-Y. Feng, S.-W. Qu, X.-H. Chen, and S. Yang, "Low-profile high-gain and wide-angle beam scanning phased transmitarray antennas," *IEEE Access*, vol. 8, pp. 34276-34285, 2020.

[9] Z.-Y. Yu, Y.-H. Zhang, S.-Y. He, H.-T. Gao, H.-T. Chen, and G.-Q. Zhu, "A wide-angle coverage and low scan loss beam steering circularly polarized folded feflectarray antenna for millimeter-wave applications," *IEEE Trans. Antennas Propag.*, vol. 70, no. 4, pp. 2656-2667, 2022.

[10] Y. Ding, S. Hou, and G. Yang, "Wide-angle scanning dielectric resonator antennas for millimeter-wave applications," *International Symposium on Antennas and Propagation (ISAP)*, pp. 1-2, 2021.

[11] Z. Qu, S. -W. Qu, Z. Zhang, S. Yang, and C. H Chan, "Wide-angle scanning lens fed by small-scale antenna array for 5G in millimeter-wave band," *IEEE Trans. Antennas Propag.*, vol. 68, no. 5, pp. 3635-3643, 2020.

[12] Y. Ye, Z. Y. Huang, Y. Jiang, L.-A. Bian, C. Zhu, J. J. Huang, and N. C. Yuan, "A wideband and wide scanning tightly coupled dipole array with metasurface wide-angle impedance matching," *Applied Computational Electromagnetics Society (ACES) Journal*, vol. 36, no. 7, pp. 872-878, 2021.

[13] Z. Zhao, Y. Zhu, and C. Deng, "Microstrip phased array antenna with small element space for 5G millimeter-wave applications," *IEEE 3rd International Conference on Electronic Information and Communication Technology (ICEICT),* pp. 620-622, 2020.

[14] S. Pan, W. Yang, W. Che, and Q. Xue, "Millimeter-wave wide-angle scanning phased array based on low-profile wide-beam patch antenna element," *IEEE MTT-S International Wireless Symposium (IWS)*, pp. 1-3, 2020.

[15] Z.-F. Yuan and Z.-H. Tu, "Wideband $\pm 45^{\circ}$ dual-polarized millimeter-wave antenna array with wide-angle scanning performance," *International Conference on Microwave and Millimeter Wave Technology (ICMMT)*, pp.1-3, 2021.

[16] M. K. Ishfaq, T. Abd Rahman, M. Himdi, H. T. Chattha, Y. Saleem, B. A. Khawaja, and F. Masud, "Compact four-element phased antenna array for 5G applications," *IEEE Access*, vol. 7, pp. 161103-161111, 2019.

[17] Y. Feng, J.-Y. Li, L.-K. Zhang, X.-J. Yu, Y.-X. Qi, D. Li, and S.-G. Zhou, "A broadband wide-angle scanning linear array antenna with suppressed mutual coupling for 5G sub-6G applications," *IEEE Antennas Wireless Propag. Lett.*, vol. 21, no. 2, pp. 366-370, 2022.

[18] X. Dai, A. Li, and K. M. Luk, "A wideband compact magnetoelectric dipole antenna fed by SICL for millimeter wave applications," *IEEE Trans. Antennas Propag.*, vol. 69, no. 9, pp. 5278-5285, Sep. 2021.

[19] Z. Tang and Y. Dong, "A Ka-band antenna array based on wide-beamwidth magnetoelectric dipole," *IEEE Antennas Wireless Propag. Lett.*, vol. 21, no. 3, pp. 501-505, 2022.

[20] J. Zeng and K. Luk, "Wideband millimeter-wave end-fire magnetoelectric dipole antenna with microstrip-line feed," *IEEE Trans. Anten-*

nas Propag., vol. 68, no. 4, pp. 2658-2665, Apr. 2020.

[21] Z. Zhou, S. Yang, and Z. Nie, "A novel broadband printed dipole antenna with low cross-polarization," *IEEE Trans. Antennas Propag.*, vol. 55, no. 11, pp. 3091-3093, Nov. 2007.

Fang-Fang Fan received a Ph.D. degree in Electromagnetic Field and Microwave Technology from Xidian University in 2011. Currently, she is an associate professor at Xidian University. Her current research interests include antenna arrays, gap waveguide technology and base station antennas for 5G application.

Qing-Lin Chen received bachelor's degree in Electronic Information Engineering from Xidian University, China, in 2020. Since 2020, he has been studying for a master's degree in Electronic and Communication Engineering at Xidian University, China. His research interests include Millimeter wave antenna array for 5G application.

Kai Qin received a master's degree from Xidian University in Xi'an, China, in June 2021. Since September 2021, he has been studying for a Ph.D. degree at City University of Hong Kong, Hong Kong, China. His research interests include antennas used in millimeter-wave and sub-Terahertz bands.